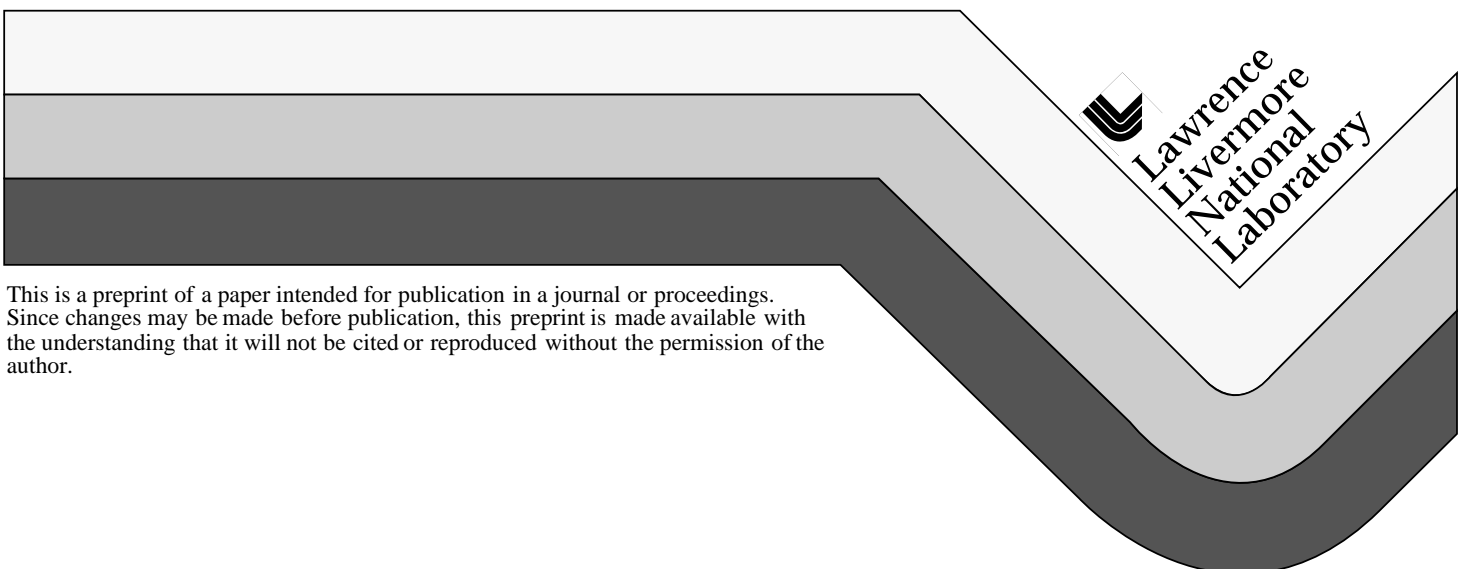# High Energy X-ray Radiography and Computed Tomography of Bridge Pins

Amy M. Waters
Harry E. Martz
Clint M. Logan
Earl Updike
Robert E. Green, Jr.

May 1999

Lawrence Livermore National Laboratory

High Energy X-ray Radiography and Computed Tomography of Bridge Pins

Amy M. Waters[1], Harry E. Martz,
Clint M. Logan and Earl Updike
Lawrence Livermore National Laboratory, L-333
7000 East Ave.
Livermore, CA 94550, USA
(925) 423-0137

Robert E. Green, Jr.
Johns Hopkins University, Center for Nondestructive Evaluation
3400 North Charles Street
Baltimore, MD 21218, USA
(410) 516-6115

Abstract

Bridge pins were used in the hanger assemblies for some multi-span steel bridges built prior to the 1980's, and are sometimes considered fracture critical elements of a bridge. During a test on a bridge conducted by the Federal Highway Administration (FHWA), ultrasonic field inspection results indicated that at least two pins contained cracks. Several pins were removed and selected for further examination. This provided an excellent opportunity to learn more about these pins and the application of x-ray systems at Lawrence Livermore National Laboratory (LLNL), as well as to learn more about the application of different detectors recently obtained by LLNL. Digital radiographs and computed tomography (CT) were used to characterize the bridge pins, using a LINAC x-ray source with a 9-MV bremsstrahlung spectrum. We will describe the performance of two different digital radiographic detectors. One is a detector system frequently used at LLNL consisting of a scintillator glass optically coupled to a CCD camera. The other detector is a new amorphous silicon detector recently acquired by LLNL.

Introduction

Bridge pins were used in the hanger assemblies for some multi-span steel bridges built prior to the 1980's, and are sometimes considered fracture critical elements of a bridge, i.e. if the element fails, the entire structure can collapse. For example, a bridge pin failure caused the 1983 collapse of the Mianus River Bridge in Connecticut that resulted in the deaths of 3 people. Bridge pin and hanger link connections used in bridges permit unrestrained movement from longitudinal expansion or contraction of adjacent spans. Typically, the upper pin penetrates the web of the cantilevered bridge girder, while the

---

[1] Graduate student at The Johns Hopkins University, Center for Nondestructive Evaluation (CNDE).

lower pin penetrates the suspended girder web. Failure of the pin or hanger generally occurs when the forces imposed on the connection exceed the strength of the pin. Factors which can influence failure include corrosion due to water or deicing chemicals used on roads, wear, fatigue cracking, or so called "frozen" connections of the assembly which result in high stresses (Gessel and Walther, 1996).

Bridge pins are typically made of steel, approximately 20 cm in length with a 7.6 cm diameter at the barrel of the pin, and threaded ends with an outer diameter of approximately 6 cm. The only part of the bridge pin accessible for inspection in the field are the exterior faces of the threaded ends. The interfaces between one girder web and the hanger plates are commonly referred to as the shear planes. The shear plane is where the shear forces from the hanger plates are transmitted to the girder web. Most defects have been found at or near the shear planes of the pins (ibid.).

Currently, bridge pins are inspected using traditional ultrasonic methods that consist of manually scanning a hand held probe over the end of a pin. Critical areas of the pin are hidden by geometric constraints, including the shear planes where most failures occur. In addition, corrosion grooves at the surfaces of the shear planes can be mistaken for cracks, and acoustic coupling between the pins and hangers can occur. Also, considering the subjective nature of the inspections, a quantitative assessment of the inspection is difficult. The Federal Highway Administration (FHWA) recently acquired several pins that had been removed from a bridge following an ultrasonic field inspection. The field study found 5 pins with significant grooves at the shear planes and 2 pins with cracks. All 7 pins were removed from the bridge and replaced. These pins were subsequently evaluated in the laboratory at FHWA using ultrasonics and high-energy radiography inspection methods. C-scans were obtained by the FHWA using an ultrasonic immersion tank and radiographs were acquired using a 6-MV betatron source with film as the detector. These lab inspection results indicated that 2 of the 7 pins contained cracks which qualitatively confirmed the field UT inspection results.

The FHWA then provided LLNL with 3 bridge pins, including the 2 cracked pins, for further evaluation using digital radiography and computed tomography. Single-view (or angle) radiography hides crucial information—that is, the overlapping of object features obscures parts of an object's features and the depth of those features is unknown. CT was developed to retrieve three-dimensional (3D) information of an obscured object's features. To make a CT measurement, several radiographic images (or projections) of an object are acquired at different angles, and the information collected by the detector is processed in a computer (Azevedo, 1991; Barrett and Swindell, 1981; Herman, 1980; Kak and Slaney, 1987). The final 3D image, generated by mathematically combining the radiographic images, provides the locations and dimensions of external and internal features of the object. Therefore, we decided to use the LLNL high-energy CT capability to better characterize the pins provided by the FHWA and to better understand the bridge pin failure mechanisms.

Experimental Method

We used a 9-MV LINAC x-ray source to penetrate the approximately 7.6 cm of steel in the bridge pins. A recently acquired dpiχ amorphous silicon (a-Si) flat panel array imager (Weisfeld, et al., 1998) was used to acquire digital radiographs and CT data for the bridge pins. The active area of the 12-bit a-Si array is 19.5 cm by 24.4 cm, with 1536 X 1920 pixels of size 127 μm. The detector requires a scintillator to convert x-rays to light before detection. An experiment was designed at LLNL to determine the optimal scintillator to use at 9 MV. The array was specially configured to evaluate 11 different materials (e.g., scintillating glass, non-scintillating glass and metal screens) and to measure x-ray sensitivity and modulation transfer functions (MTFs) for each material/detector combination. It was determined that MinR provided the best MTF at 9-MV of all the materials tested. MinR is an inexpensive, commercially available scintillating screen commonly used in film/screen mammography at low energies. The scintillator material is GdO_2S_2, it is well characterized and consistently manufactured, and produces a high-spatial resolution with a uniform response. MTFs were measured at 9-MV for the MinR/dpiχ array compared to two scintillator/lens/CCD detector systems frequently used at LLNL (Fig. 1). The scintillators are high-density terbium oxide doped glass. We evaluated both a 6-mm thick glass plate and a 12-mm thick fiber-optic glass plate.
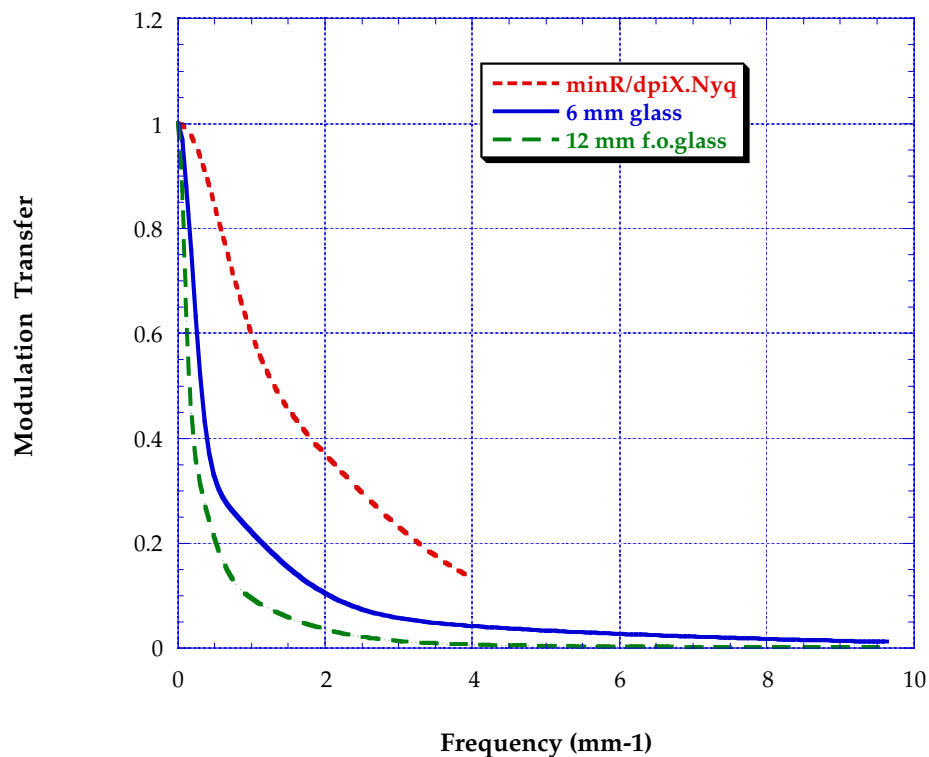

Fig. 1 Modulation Transfer Functions (MTF) of a radiographic 3.175 mm thick depleted-U edge for the MinR/dpiχ detector system and two scintillator/lens/CCD detector systems at LLNL.

The MinR/dpiχ detector outperformed the scintillating glasses in x-ray sensitivity and by a factor of almost 4 times better spatial response at 2 lp/mm at 9-MV. Therefore we decided to use the MinR/dpiχ detector system to acquire the 9-MV digital radiographs of all three bridge pins, two cracked pins and one uncracked pin. The source was located approximately 5.08 m (16.6 ft) from the pins, and the detector was located approximately 0.1 m (4 in) behind the bridge pin. CT data was acquired for the cracked pin only and consisted of 180 projections over 180 degrees. Due to the large amount of data from the CT acquisition, the CT data from the cracked pin was extracted down to the area surrounding the crack. The projections were reconstructed along the longitudinal, or z, axis using a convolution back projection (CBP) algorithm into 200 slices or tomograms of 760 x 760 pixels with a volume element (voxel) size of 127x127x127 μm^3. The data was then merged into a 3-dimensional volume (760 x 760 x 200) for further analysis along the x and y axes.

Results/Analysis
Digital radiographs of the three pins are shown in Figure 2. The pin on the far left shows no visible grooves or cracks. This pin was removed from the bridge after field UT revealed significant grooves at the shear planes. This was confirmed by visual inspection. The pin in the center shows grooves at the shear planes, particularly the lower shear plane, while the pin on the right clearly shows a large crack at the upper shear plane. Field UT results revealed that both of these pins contained cracks.
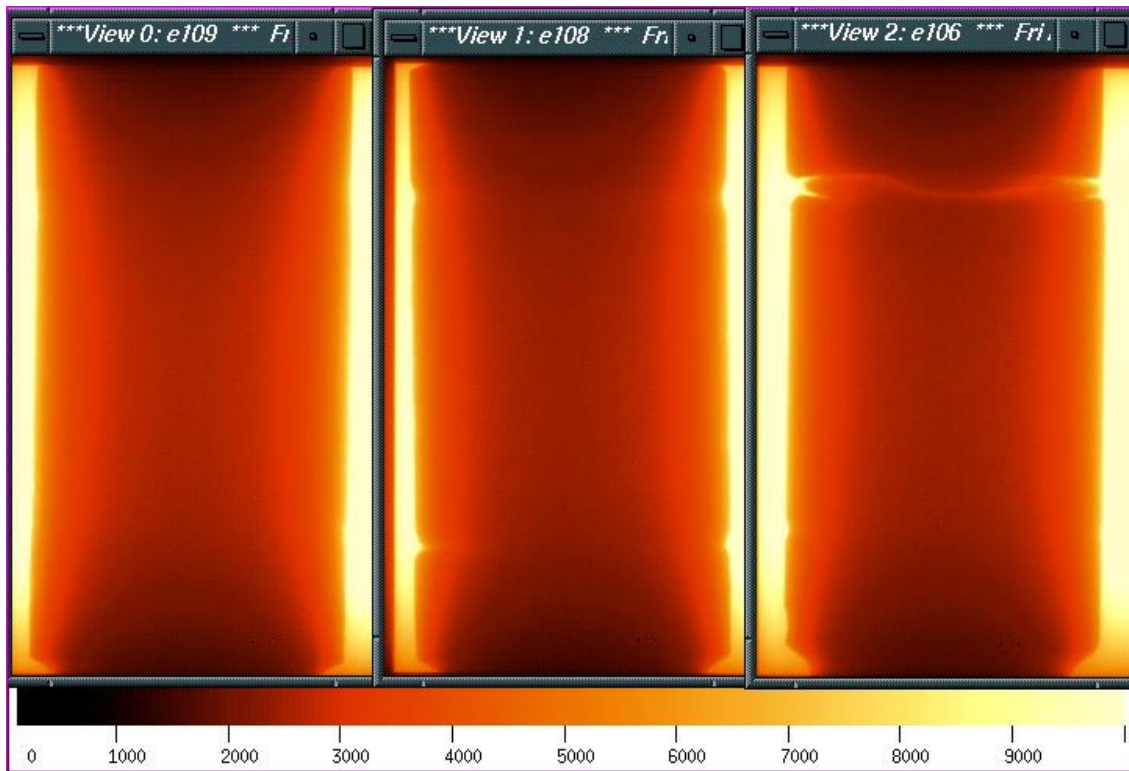

Fig. 2. Digital radiographs of three bridge pins provided by FHWA. From left to right: uncracked pin, slightly cracked pin, and severely cracked pin.
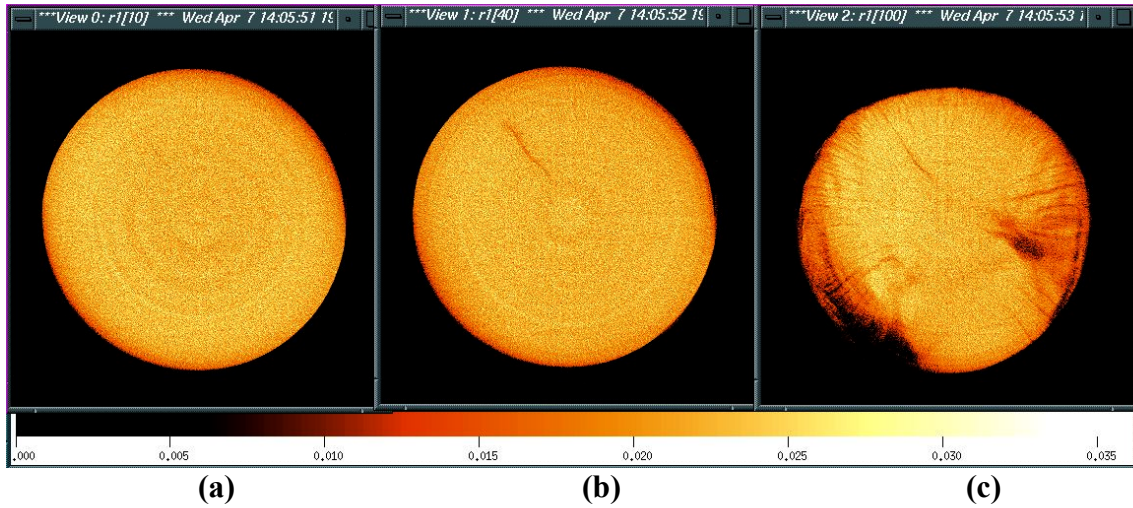
Fig. 3 Tomograms along the longitudinal axis of a cracked bridge pin. The tomograms are (a) far from (b) near and (c) within the cracked shear plane region. The gray scale relates gray tones to relative linear attenuation in mm^{-1} units.

Three representative tomograms along the longitudinal (or z) axis from the cracked pin are shown in Figure 3. Figure 3(a) is a slice far (~11 mm) above the shear plane region of the pin. Note the uniform appearance of the pin, i.e. no apparent cracks or voids. Closer (~8 mm) to the shear plane, Fig. 3(b), note the radial crack located in the upper left quadrant. It is useful to note that these radial cracks, which run along the longitudinal, or z axis, do not appear at distances greater than 11 mm from the shear plane. The radial crack seen in Fig. 3(b) is also seen in Fig. 3(c) along with additional radial cracks, and there is a large breaking crack through the shear plane. This slice is taken within the shear plane. The large shear plane cracks were also seen using lab UT methods and visual inspection.

Two representative CT slices along the y axis are shown in Figure 4. Note the longitudinal radial cracks are clearly visible in the region above, through and below the large shear plane crack in the slice on the left. This seems to imply that the radial cracks contribute to the overall shear plane cracking and eventual failure of the pin. Radial cracks were not observed using UT methods or visual inspections. The slice on the right clearly shows that the shear plane crack penetrates almost to the center of the pin. This data can be used to quantify crack size and dimensions.
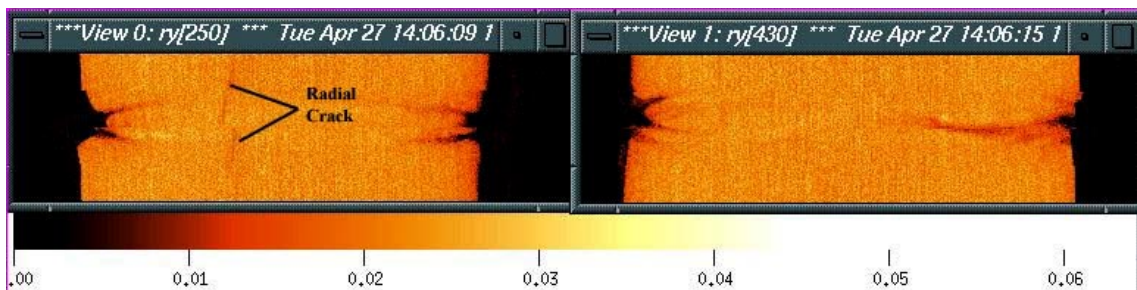

Fig. 4 CT slices along the y axis of the cracked bridge pin. Note the slice on the left reveals a longitudinal radial crack above, through and below the large shear plane crack.

Summary/conclusions/future work

A new a-Si detector system (MinR/dpiχ) was used to acquire digital radiographs for three bridge pins and computed tomography data for one cracked bridge pin. The a-Si detector results are very promising for large fields of view. Computed tomography reveals many more internal defects within the bridge pins that were not observed with other NDE inspection methods such as visual, radiographic, or ultrasonic methods. For example, we observed radial cracks running longitudinally above, through and below the large shear plane crack, which possibly contribute to pin failure and we are able to quantitatively measure cracking in three dimensions. To the first order the field and laboratory ultrasonic inspection results were corroborated by the CT data showing large shear plane cracks. This provides some level of confidence in the ultrasonic field inspection method, but further work is required to quantitatively correlate the UT data with the x-ray tomographic data. In addition, further studies are required to better understand the failure mechanisms in bridge pins, for example the effect of radial cracking on the shear plane failures. Also, more tests are needed to determine the performance of the a-Si detector systems.

References

Azevedo, S. G., 1991. Model-Based Computed Tomography for Nondestructive Evaluation. Ph.D. Dissertation. Lawrence Livermore National Laboratory, Livermore, Calif., UCRL-LR-106884, March.

Barrett, H. H., and W. Swindell, 1981. Radiological Imaging: Theory of Image Formation, Detection, and Processing, vols. 1 and 2. New York: Academic Press.

Gessel, R. D., and R. A. Walther, 1996. "Ultrasonic Inspection of Bridge Pin and Hanger Assemblies," *Structural Materials Technology, Proceedings*. Lancaster, PA: Technomic Publishing.

Herman, G. T., 1980. Image Reconstruction from Projections: The Fundamentals of Computerized Tomography. New York: Academic Press.

Kak, A. C., and M. Slaney, 1987. Principles of Computerized Tomographic Imaging. New York: IEEE Press.

Weisfeld, R. L., Hartney, M. A., Street, R. A., and Apte, R. B., 19098. "New Amorphous-Silicon Image Sensor for X-Ray Diagnostic Medical Imaging Applications," *SPIE Medical Imaging, Physics of Medical Imaging*, vol. 3336, pp. 444-452.